JOURNAL OF CHEMICAL INFORMATION AND MODELING

Article

pubs.acs.org/jcim

Acetylcholinesterase Inhibitors: Structure Based Design, Synthesis, Pharmacophore Modeling, and Virtual Screening

Koteswara Rao Valasani,[†] Michael O. Chaney,[†] Victor W. Day,[‡] and Shirley ShiDu Yan*[,†]

[†]Department of Pharmacology & Toxicology and Higuchi Bioscience Center, School of Pharmacy, and [‡]Department of Chemistry, University of Kansas, Lawrence, Kansas 66047, United States

Supporting Information

ABSTRACT: Acetylcholinesterase (AChE) is a main drug target, and its inhibitors have demonstrated functionality in the symptomatic treatment of Alzheimer's disease (AD). In this study, a series of novel AChE inhibitors were designed and their inhibitory activity was evaluated with 2D quantitative structure−activity relationship (QSAR) studies using a training set of 20 known compounds for which IC_{50} values had previously been determined. The QSAR model was calculated based on seven unique descriptors. Model validation was determined by predicting IC_{50} values for a test set of 20 independent compounds with measured IC_{50} values. A correlation analysis was carried out comparing the statistics of the measured IC_{50} values with predicted ones. These selectivity-determining descriptors were interpreted graphically in terms of principal component analyses (PCA). A 3D pharmacophore model was also created based on the activity of the training set. In addition, absorption, distribution, metabolism, and excretion (ADME) descriptors were also determined to evaluate their pharmacokinetic properties. Finally, molecular docking of these novel molecules into the AChE binding domain indicated that three molecules (**6c**, **7c**, and **7h**) should have significantly higher affinities and solvation energies than the known standard drug donepezil. The docking studies of 2*H*-thiazolo[3,2-*a*]pyrimidines (**6a**−**6j**) and 5*H*-thiazolo[3,2-*a*] pyrimidines (**7a**−**7j**) with human AChE have demonstrated that these ligands bind to the dual sites of the enzyme. Simple and ecofriendly syntheses and diastereomeric crystallizations of 2*H*-thiazolo [3,2-*a*]pyrimidines and 5*H*-thiazolo[3,2-*a*] pyrimidines are described. The solid-state structures for the HBr salts of compounds **6a**, **6e**, **7a**, and **7i** have been determined using single-crystal X-ray diffraction techniques, and X-ray powder patterns were measured for the bulk solid remaining after solvent was removed from solutions containing **6a** and **7a**. These studies provide valuable insight for designing more potent and selective inhibitors for the treatment of AD.

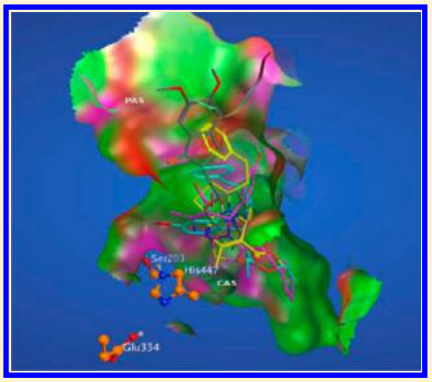

1. INTRODUCTION

Alzheimer's disease (AD) is the most common cause of dementia in adults, resulting in a disorder of cognition and memory due to neuronal stress and eventually in cell death. Alzheimer brain is characterized by two pathological features: amyloid beta (Aβ) accumulation and the formation of neurofibrillary tangles. Accumulation of Aβ is considered to be one of the primary causes for the AD pathogenesis. Scientists have proposed several hypotheses for AD development.[1−9] One of the oldest AD hypotheses, the cholinergic hypothesis,[10] has led to the development of cholinesterase inhibitors (ChEIs) that increase levels of acetylcholine (ACh) through inhibition of cholinesterases (ChEs).[11] The most predominant hypothesis, the amyloid hypothesis,[12,13] postulates that increased production of β-amyloid peptide and its aggregation and accumulation in the brain lead to neuronal cell death. Since it is known that ACh deficiency is associated with AD,[14] inhibiting the biological activity of ChEs to increase ACh levels in the brain is one of the major therapeutic strategies for the treatment of AD. Acetylcholinesterase (AChE) inhibitors are the most frequently prescribed drugs for AD, which promote memory function and delay the cognitive decline without altering the underlying pathology.

The deficiencies in cholinergic neurotransmission in AD have led to the development of potent AChE inhibitors (AChEIs). A large number of naturally occurring and synthetic AChE inhibitors have already been identified[15,16] as the first-line treatment for symptoms of this disease and are prescribed for mild-to-moderate AD. Four AChEIs have been approved by the United States FDA and many other jurisdictions for the treatment of AD:[17−19] tacrine, donepezil, rivastigmine, and galantamine. Tacrine is no longer in general use because of dosing, tolerability, and safety concerns. The clinical benefits of these agents include improvements, stabilization, or less-than-expected decline in cognition and other mental function. Slightly different mechanisms of action have been reported for the available inhibitors. They appear to affect the ease of use and tolerability more than drug effectiveness though, since neither systematic reviews, nor head-to-head studies, identify significant efficacy differences between the agents.[20−22]

Received: April 2, 2013
Published: June 18, 2013

Subsequent clearly reported, carefully conducted, systematic, evidence-based reviews of these agents are available.[20,23−25] It is important to understand that none of these medications stop the disease itself. At best, they only slow progression and do not appear to affect the basic destructive disease process. When patients go off the drugs, the deterioration continues.

Although all of the FDA-approved Alzheimer's medicines have, in general, been shown to *somewhat* improve a patient's well-being, most patients will not experience *significant* improvement. Studies have shown that only about 10% of patients are considered to be "better" when assessed by their doctor or caregiver. The remaining 90% may not decline as much as they would have without drug treatment but overall *improvement* will likely not be noted. While head-to-head studies of the various medicines could provide meaningful comparisons for some aspects of AD treatment, it is difficult to make head-to-head comparisons in their ability to improve overall well-being.

The 3D structure of AChE from native *Torpedo californica* (TcAChE) has been determined by X-ray crystallography (Protein Data Bank, PDB code: 2ACE)[26] and is similar to the structure of human AChE (*h*AChE). Both molecules are α/β serine hydrolases with 537 residues and a 12-stranded mixed β sheet surrounded by 14 α helices. The active sites in both crystal structures are also similar. Docking simulations were performed to gain insight into the recognition between the AChE and the ligands. For *Tc*AChE, these experiments indicated that recognition occurred in a deep, narrow groove approximately 20 Å long on the enzyme surface. For TcAChE, this groove contains both the catalytic active site (CAS) with the Ser-His-Glu catalytic triad (Ser203-His447-Glu334) and the peripheral anionic site (PAS) that utilizes Trp86, Tyr133, Glu202, Phe338, and Tyr449. A substantial portion of the surface of this groove is lined by fourteen highly conserved aromatic residues. The PAS is located at the aromatic-lined entrance of the groove. This aromatic lined-entrance contains Tyr72, Tyr124, Trp279, and Tyr337 residues.[27] Reversible inhibitors bind to the CAS or to the PAS and dimeric (dual) inhibitors bind simultaneously to both of the sites. Noncatalytic roles of AChE have been established in the past decade. AChE has been shown to play a key role in the acceleration of amyloid β (Aβ)-peptide deposition and promoting the formation of amyloid β-plaques.[27] Dual-binding AChE inhibitors which bind to PAS have been shown to inhibit such processes.[28] A single molecule can therefore serve two important biological roles.

Further studies indicated that the hydrophobic environment close to the PAS promotes the interaction of AChE with Aβ-peptide to form Aβ fibrils that lead to neurotoxicity.[29,30] These reports suggest that AChEIs enhance the release of non-amyloidogenic soluble derivatives of amyloid precursor protein (APP) both in vitro and in vivo, thereby slowing the formation of amyloidogenic compounds in the brain.[31] AChEIs also increase the solubility of APP.[32] Numerous clinical trials have revealed the safety and efficacy of AChEIs in the treatment of AD. Preclinical studies suggested that these AChEIs also attenuate neuronal cell death from neuronal cytotoxicity and therefore provide another treatment for AD.[33]

Since it was also discovered that AChE augments the neurotoxic effect of Aβ peptide by accelerating the formation of beta amyloid deposits in the brain, the role of Aβ peptide at the onset and during progression of AD is a matter of debate.[34,35] It is well-known that the enzyme interacts with beta amyloid through the PAS and promotes the formation of fibrils.[36] We have therefore focused on developing compounds that are able to interact with both the CAS and PAS of AChE as a potentially new therapeutic approach for the effective management of AD symptoms.[32,37]

Pyrimidine derivatives are widely used as treatment of AD at different stages,[38−41] and they have previously been reported to be useful as gamma secretase modulators,[42] treatments for diseases like AD associated with the deposition of beta-amyloid peptide in the brain,[39] inhibitors for microtubule affinity regulating kinases,[43] or compounds for the treatment or prevention of tauopathies.[44]

Since pyrimidines are also components or building blocks for the synthesis of many important biologically active compounds[45,46] and the groove of AChE is lined with a high percentage of aromatic side chains, we concentrated on synthesizing molecules with aromatic side chains attached to a pyrimidine moiety. Herein, we report the design, molecular docking studies, quantitative structure−activity relationship (QSAR) studies, preADME (absorption, distribution, metabolism, and excretion) predictions, 3D pharmacophore modeling results, synthesis, diastereomeric crystallization, single crystal X-ray diffraction (XRD) and powder XRD for AChEIs of pyrimidine derivatives.

2. MATERIALS AND METHODS

Construction of a 2D QSAR Model.[47] The QSAR suite of applications in MOE was used to calculate and analyze the data and build numerical models of the data for prediction and interpretation purposes. Any QSAR model for a given set of molecules correlates the activities with properties inherent to each molecule in the set itself. A database of 40 compounds with known IC_{50} values was used to generate independent training and test data sets. Initially, a total of seven QSAR descriptors were defined for the training set compounds to carry out a correlation analysis and to construct the QSAR model based on these properties. These descriptors are all independent variables and the IC_{50} values of the each compound were considered as dependent variable to predict the activity of each test set compound.

Fitting the Experimental Data. The predicted activities were chosen as dependent variable in the test data set and a QSAR model was constructed choosing this predicted activity and the remaining descriptors as model fields. Regression analysis was performed for the training data set and root mean square error (RMSE) and r^2 values of the fit were reported. This fit model was saved as the QSAR model and used for the prediction of activities of compounds of test data set.

Cross-Validating the Model. The above QSAR fit was used for both model validation and cross-validation. This validation procedure will evaluate the predicted activities and the residuals for the training set molecules. The predicted, residual, and *Z*-score values were calculated for both model and cross-validations.

Graphical Analysis. The predictive ability of the model was assessed using a correlation plot by plotting the predicted ($PRED) values (*X*-axis) versus the predicted IC_{50} activities (*Y*-axis). This correlation plot was used to identify outliers that have a *Z*-score beyond the range of 2.

Estimation and Validation of Predicted Activities of Test Set. The QSAR model fit obtained above was used to evaluate the predicted (PRED Activity) values of 20 test set compounds. Regression analysis was performed for the test data

Table 1. Crystal Data and Details of the Structure Determination for 6a and 6e

identification code	6a	6e
empirical formula	$C_{24}H_{26}BrN_3O_5S$	$C_{26}H_{29}BrN_2O_6S$
formula weight	548.45	577.48
temperature	100(2) K	100(2) K
wavelength	1.54178 Å	1.54178 Å
crystal system	monoclinic	monoclinic
space group	$P2_1/n$ [an alternate setting of $P2_1/c$ – C_{2h}^5 (no. 14)]	$P2_1/c$
unit cell dimensions	a = 11.8312(3) Å α = 90.000°	a = 17.3323(4) Å α = 90.000°
	b = 14.0673(4) Å β = 101.301(1)°	b = 9.4672(3) Å β = 110.0380(10)°
	c = 14.5827(4) Å γ = 90.000°	c = 17.1701(4) Å γ = 90.000°
volume	2380.0(1) Å^3	2646.9(1) Å^3
Z	4	4
density (calculated)	1.531 g/cm^3	1.449 g/cm^3
absorption coefficient	3.527 mm^{-1}	3.218 mm^{-1}
F(000)	1128	1192
crystal size	0.12 mm × 0.11 mm × 0.06 mm	0.08 mm × 0.03 mm × 0.03 mm
theta range for data collection	4.41–69.76°	2.71–70.00°
index ranges	$-14 \le h \le 14$, $-16 \le k \le 16$, $-17 \le l \le 14$	$-20 \le h \le 20$, $-11 \le k \le 11$, $-20 \le l \le 20$
reflections collected	22191	23911
independent reflections	4389 [R_{int} = 0.019]	4887 [R_{int} = 0.041]
completeness to theta = 66.00°	99.7%	99.7%
absorption correction	multiscan	multiscan
max. and min transmission	1.000 and 0.808	1.000 and 0.881
refinement method	full-matrix least-squares on F^2	full-matrix least-squares on F^2
data/restraints/parameters	4389/0/411	4887/0/441
goodness-of-fit on F^2	1.102	1.045
final R indices [$I > 2\sigma(I)$]	R_1 = 0.026, wR_2 = 0.068	R_1 = 0.035, wR_2 = 0.085
R indices (all data)	R_1 = 0.026, wR_2 = 0.069	R_1 = 0.038, wR_2 = 0.086
largest diff. peak and hole	0.48 and −0.30 e$^-$/Å^3	0.82 and −0.50 e$^-$/Å^3

set and root mean square error (RMSE) and r^2 values of the fit were reported.

Pruning the Descriptors. Pruning the descriptors is necessary to select the optimum set of molecules under consideration. "QuaSAR-Contingency", a statistical application in MOE was used to describe the best molecules in the data set. The results were analyzed using principal component analysis (PCA), the purpose of which is to reduce the dimensionality of set of molecular descriptors by linearly transforming the data or defying a property that would be important to drug design. A three-dimensional scatter graphical plot was generated using the first three principal components (PCA1, PCA2, and PCA3).

ADMET Prediction.[48,49] Absorption, distribution, metabolism, excretion, and toxicity (ADMET) properties of the 20 novel compounds were calculated using the preADMET online server (http://preadmet.bmdrc.org/). The ADMET properties, human intestinal absorption, in vitro Caco-2 cell permeability, in vitro Maden Darby Canine Kidney (MDCK) cell permeability, in vitro plasma protein binding, and in vivo blood brain barrier penetration were predicted using this program.

Molecular Docking.[50,51] *Preparation of AChE Protein.* The three-dimensional structure of AChE was retrieved from the Protein Data Bank (PDB http://www.rcsb.org/pdb, PDB ID 1B41) and loaded into the MOE software. All water molecules and heteroatoms were removed, and polar hydrogens were added. Protonation of the 3D structure was done for all the atoms in implicit solvated environment (Born solvation model) at a specified temperature of 300 K, pH of 7, and with a salt concentration value of 0.1. A nonbonded cut off value of 10–12 Å was applied to the Leonard-Jones terms. After the protonation, the complete structure was Energy minimized in MMFF94x force field at a gradient cut off value of 0.05. Molecular dynamics simulations were carried out at a constant temperature of 300 K for a heat time of 10 ps. The total simulations were carried out for a total period of 10 ns. The time step was considered as 0.001, and the temperature relaxation time was set to 0.2 ps. The position, velocity, and acceleration were saved every 0.5 ps.

Prediction of Binding Site for Ligands. The binding site for docking of our ligand candidates was defined by the donepezil inhibitor obtained from the AChE crystal structure (PDB http://www.rcsb.org/pdb, PDB ID 1B41). The donepezil molecule was obtained from the AChE crystal structure (PDB http://www.rcsb.org/pdb, PDB ID 4EY7). It was positioned into the 1B41 structure by alignment and superposition of the two proteins. The docking routine within MOE allows the user to define a binding region from the donepezil molecule. In our case we used $r \le 10$ Å.

Molecular Docking.[52] The ligand database generated from the list of all novel ligand molecules was docked into the specified binding domain of the AChE receptor using alpha PMI (Principal Moments of Inertia) placement methodology where poses are generated by aligning ligand conformations principal moments of inertia to a randomly generated subset of alpha spheres in the receptor site. Thirty docked conformations were generated for each ligand and ranked by alpha HB scoring function which is a linear combination of the geometric fit of the ligand to the binding site and hydrogen bonding effects. From all the receptor–ligand complexes, the conformation with the lowest docking score was chosen for the analysis.[57] The interaction of all ligand molecules in the binding domain cavity was analyzed from ligand interaction study of MOE.[5] The ligand–receptor complexes were analyzed by both London ΔG free energy approximations and interaction energies, ΔE.

Pharmacophore Model. A pharmacophore defines both features and locations of important binding interactions between a ligand and its receptor. Our pharmacophore model was constructed by overlapping the top six ligand candidates that calculated with the strongest binding affinity. The Unified scheme within MOE was used to define the features thought to be important for ligand binding. The locations of these features were determined by inspection of strong interactions of the ligands with the AChE receptor.

Chemistry. *General.* All reagents were commercially available and used without further purification. Melting points were determined in open capillary tubes on a Laboratory

Table 2. Crystal Data and Details of the Structure Determination for 7a and 7i

identification code	7a		7i	
empirical formula	$C_{24}H_{24}BrN_3O_4S$		$C_{46}H_{46}Br_2N_4O_6S_2$	
formula weight	530.43		974.81	
temperature	100(2) K		100(2) K	
wavelength	1.54178 Å		1.54178 Å	
crystal system	triclinic		monoclinic	
space group	$P\bar{1}-C_i^1$ (no. 2)		$P2_1/c$	
unit cell dimensions	a = 6.9449(2) Å	α = 63.855(1)°	a = 13.519(2) Å	α = 90.000°
	b = 13.1458(3) Å	β = 82.550(1)°	b = 18.428(3) Å	β = 90.674(3)°
	c = 14.5214(4) Å	γ = 77.793(1)°	c = 17.734(3) Å	γ = 90.000°
volume	1162.19(5) Å^3		4417.6(12) Å^3	
Z	2		4	
density (calculated)	1.516 g/cm^3		1.466 mg/m^3	
absorption coefficient	3.559 mm^{-1}		3.642 mm^{-1}	
F(000)	544		2000	
crystal size	0.08 mm × 0.07 mm × 0.04 mm		0.23 mm × 0.12 mm × 0.11 mm	
theta range for data collection	3.39−69.84°		3.27−68.06°	
index ranges	$-8 \le h \le 8$, $-15 \le k \le 15$, $-15 \le l \le 17$		$-16 \le h \le 13$, $-22 \le k \le 21$, $-21 \le l \le 20$	
reflections collected	10712		28150	
independent reflections	4023 [R_{int} = 0.014]		7814 [R_{int} = 0.022]	
completeness to theta =66.00°	95.2%		99.2%	
absorption correction	multiscan		multiscan	
max. and min transmission	1.000 and 0.891		1.000 and 0.630	
refinement method	full-matrix least-squares on F^2		full-matrix least-squares on F^2	
data/restraints/parameters	4023/0/394		7814/0/686	
goodness-of-fit on F^2	1.070		1.076	
final R indices [$I > 2\sigma(I)$]	R_1 = 0.023, wR_2 = 0.060		R_1 = 0.035, wR_2 = 0.094	
R indices (all data)	R_1 = 0.024, wR_2 = 0.060		R_1 = 0.035, wR_2 = 0.094	
largest diff. peak and hole	0.54 and −0.29 e$^-$/Å^3		0.69 and −0.55 e$^-$/Å^3	

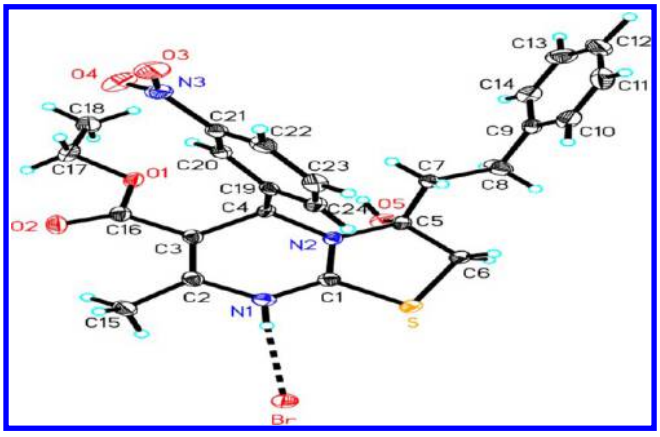

Figure 1. Crystal structure for HBr salt of **6a** showing 50% probability displacement ellipsoids and atom-numbering scheme.

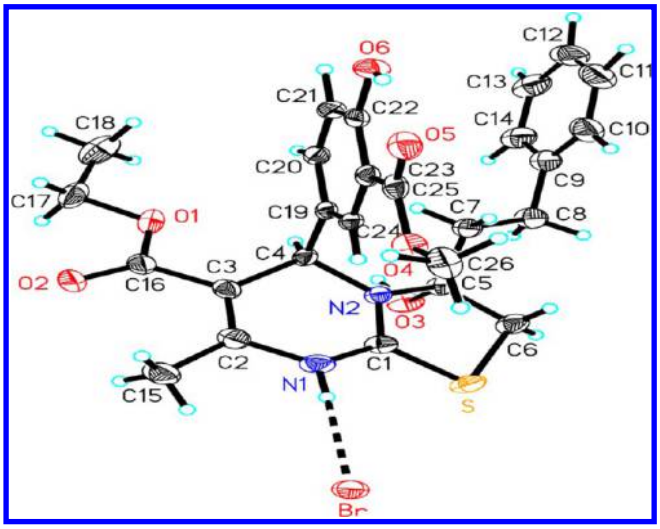

Figure 2. Crystal structure for HBr salt of **6e** showing 50% probsability displacement ellipsoids and atom-numbering scheme.

Devices Mel-Temp apparatus and are uncorrected. ^{1}H and ^{13}C NMR spectra were recorded in d_6-DMSO on a Bruker DRX-500 spectrometer operating at 500 and 125 MHz, respectively, and calibrated to the solvent peak. Abbreviations used for the split patterns of proton NMR signals are singlet (s), doublet (d), triplet (t), quartet (q), quintet (qui), multiplet (m), and broad signal (br). High-resolution mass spectrometry (HRMS) was recorded on a LCT Premier Spectrometer.

*Synthesis of Methyl 4-(4-Hydroxy-3-(methoxycarbonyl) phenyl)-6-methyl-2-thioxo-1,2,3,4-tetrahydropyrimidine-5-carboxylate (**4e**).* To a stirred solution of ethyl acetoacetate (1 mmol), methyl 5-formyl-2-hydroxybenzoate (1 mmol) and thiourea (1 mmol) in ethanol (10 mL) were refluxed in the presence of poly phosphoric acid (1 mmol %) for 8 h. The progress of the reaction was monitored by thin layer chromatography (TLC; dichloromethane:ethyl acetate, 1:1 v/v). After completion of the reaction, the reaction mixture was cooled to room temperature, and it was poured into crushed ice (20 g) and formed the white solid. The solid was filtered under suction, washed with ice-cold water, and then recrystallized from hot ethanol to afford the methyl 4-(4-hydroxy-3-(methoxycarbonyl) phenyl)-6-methyl-2-thioxo-1,2,3,4-tetrahydropyrimidine-5-carboxylate (**4e**), white crystals. Yield: 87%.

dx.doi.org/10.1021/ci400196z | J. Chem. Inf. Model. 2013, 53, 2033−2046

Mp: 211−213 °C. R_f 0.32 (dichloromethane:ethyl acetate, 1:1 v/v). IR: 3344, 3238, 2974, 2883, 1924, 1714, 1668, 1568, 1527, 1348, 1253, 881, 736, 698 cm^{-1}. ^1H NMR (DMSO-d_6) δ 2.30 (s, 3H), 3.55 (s, 3H), 3.89 (s, 3H), 5.14 (d, J = 5.0 Hz, 1H), 6.98−7.00 (m, 1H), 7.33−7.35 (m, 1H), 7.64 (d, J = 5.0 Hz, 1H), 9.63−9.66 (m, 1H), 10.36−10.39 (m, 1H), 10.49 (s, 1H). ^{13}C NMR (DMSO-d_6) δ 13.9, 17.2, 51.1, 52.5, 53.2, 59.6, 100.1, 112.9, 117.8, 127.9, 133.6, 134.2, 145.4, 159.4, 165.5, 168.8, 173.9.

The same experimental procedure was adopted for the preparation of the remaining title compounds **4a**−**4j**.

*Ethyl 4-(4-Hydroxy-3-(methoxycarbonyl) phenyl)-6-methyl-2-thioxo-1,2,3,4-tetrahydropyrimidine-5-carboxylate (**4j**).* White crystals, 84% yield. Mp: 239−241 °C. R_f 0.30 (dichloromethane:ethyl acetate, 1:1 v/v). Yield: 82%. IR: 3330, 3236, 2927, 2883, 1924, 1714, 1668, 1568, 1525, 1346, 1253, 1091, 1051, 881, 738, 698 cm^{-1}. ^1H NMR (DMSO-d_6) δ 1.11 (t, 3H), 2.29 (s, 3H), 3.89 (s, 3H), 3.96−4.06 (m, 2H), 5.14 (d, J = 5.0 Hz, 1H), 6.99 (d, J = 10.0 Hz, 1H), 67.34 (m, 1H), 7.65 (d, 1H), 9.63−9.64 (m, 1H), 10.36 (d, 1H), 10.48 (s, 1H). ^{13}C NMR (DMSO-d_6) δ 13.9, 17.1, 52.5, 53.3, 59.6, 100.4, 112.8, 117.9, 127.9, 133.6, 134.6, 145.1, 159.3, 164.9, 168.8, 173.9. HRMS cald for $C_{16}H_{18}N_2O_5S$ (M + H) 350.0936; found 453.0900 (TOF MS ES$^+$).

*Synthesis of Ethyl 3-Hydroxy-7-methyl-5-(3-nitrophenyl)-3-phenethyl-3,5-dihydro-2H-thiazolo[3,2-a]pyrimidine-6-carboxylate (**6a**).* To a solution of ethyl 6-methyl-4-(3-nitrophenyl)-2-thioxo-1,2,3,4-tetrahydropyrimidine-5-carboxylate (**4a**) (1 mmol) in water (5 mL) and tetrahydrofuran (2.5 mL), 1-bromo-4-phenylbutan-2-one (1 mmol) was added to this solution, and the reaction mixture was stirred for 8 h at room temperature. The progress of the reaction was monitored by TLC (dichloromethane:ethylacetate 1:1). After completion of the reaction, a white solid was formed. The solid was filtered off and washed with water and dried. The solid was recrystallized from methanol to get the pure product of ethyl 3-hydroxy-5-(4-hydroxy-3-(methoxycarbonyl) phenyl)-7-methyl-3-phenethyl-3,5-dihydro-2*H*-thiazolo[3,2-*a*]pyrimidine-6-carboxylate (**6a**). Colorless solid, R_f 0.37 (dichloromethane:ethyl acetate, 1:1 v/v). Yield: 83%. Mp: 217−220 °C. IR: 3232, 2902, 2864, 2690, 2362, 1712, 1666, 1569, 1529, 1350, 1259, 1091, 748, 703 cm^{-1}. ^1H NMR (DMSO-d_6) δ 1.18 (t, 3H), 2.27 (s, 3H), 2.39 (s, 2H), 2.67−2.85 (m, 2H), 3.54−3.58 (m, 1H), 3.96−4.19 (m, 3H), 5.80 (s, 1H), 6.922−6.95 (m, 1H), 7.12−7.32 (m, 5H), 7.64−7.70 (m, 1H), 7.78−7.89 (m, 1H), 8.14−8.20 (m, 2H). ^{13}C NMR (DMSO-d_6) δ 13.8, 17.7, 28.9, 36.8, 37.7, 48.6, 54.3, 54.8, 60.7, 105.1, 122.3, 123.2, 123.7, 126.2, 127.7, 128.2, 128.4, 130.7, 140.0, 143.8, 147.4, 147.6, 163.4, 166.6. HRMS cald for $C_{24}H_{26}N_3O_5S$ (M + H) 468.1593; found 468.1574 (TOF MS ES$^+$).

The same experiment procedure was followed for the remaining title compounds **6b**−**6j.**

*Synthesis of Ethyl 7-Methyl-5-(3-nitrophenyl)-3-phenethyl-5H-thiazolo[3,2-a]pyrimidine-6-carboxylate (**7a**).* Ethyl 3-hydroxy-7-methyl-5-(3-nitrophenyl)-3-phenethyl-3,5-dihydro-2*H*-thiazolo[3,2-*a*]pyrimidine-6-carboxylate (1 mmol) in water (5 mL) and ethanol (3 mL) was taken in a reaction flux and refluxed for 6 h. The progress of the reaction was monitored by TLC (dichloromethane:ethylacetate 1:1). After completion of the reaction, the solvent was removed under reduced pressure. The solid was recrystallized from methanol to afforded the title compound methyl 7-methyl-5-(3-nitrophenyl)-3-phenethyl-5*H*-thiazolo[3,2-*a*]pyrimidine-6-carboxylate (**7a**). Colorless solid, R_f 0.40 (dichloromethane:ethyl acetate, 1:1 v/v). Yield: 81%. Mp: 236−238 °C. IR: 3055, 2981, 2894, 2684, 2360, 1683, 1591, 1527, 1348, 1110, 1010, 748 cm^{-1}. ^1H NMR (DMSO-d_6) δ 1.22 (*t*, 3H), 2.40 (*s*, 3H), 2.63−2.71 (m, 2H), 2.78−2.84 (m, 1H), 3.07−3.13 (m, 1H), 4.01−4.19 (m, 2H), 6.64 (s, 1H), 7.09−7.25 (m, 6H), 7.71 (t, 1H), 7.78−7.80 (m, 1H), 8.21−8.25 (m, 2H). ^{13}C NMR (DMSO-d_6) δ 13.9, 18.3, 27.2, 32.0, 57.5, 60.6, 101.5, 108.7, 122.1, 124.1, 126.3, 128.2, 128.3, 131.1, 133.6, 139.4, 140.6, 141.7, 147.8, 161.4, 163.7. HRMS cald for $C_{24}H_{24}N_3O_4S$ (M + H) 450.1488; found 450.1475 (TOF MS ES$^+$).

The same experimental method was adopted for the preparation of the remaining title compounds (**7b**−**7j**).

*Powder Pattern and Single Crystal Structure Comparison for Compound **6a**.* Room temperature X-ray powder patterns were obtained using monochromated Cu Kα radiation (λ = 1.54178 Å) on a Bruker Proteum Diffraction System equipped with Helios multilayer optics, an APEX II CCD detector, and a Bruker MicroStar microfocus rotating anode X-ray source operating at 45 kV and 60 mA. The powders were mixed with a small amount of Paratone N oil to form a paste that was then placed in a small (<0.5 mm) nylon kryoloop and mounted on a goniometer head. The specimen was then positioned at the goniometer center-of-motion by translating it on the goniometer head. Three overlapping 1 min 180° φ-scans were collected using the Bruker Apex2 V2010.3-0 software package[53] with the detector at 2θ = 30°, 60°, and 90° using a sample-to-detector distance of 50.0 mm. These overlapping scans were merged and converted to a RAW file using the Pilot/XRD2 evaluation option that is part of the APEX2 software package. This RAW file was then processed using the Bruker EVA powder diffraction software package.

Crystal Data and Structure Determination of the Synthesized Compound. Colorless single-domain crystals of 2*H*-thiazolo[3,2-*a*]pyrimidines (**6a**) and (**6e**) and 5*H*-thiazolo-[3,2-*a*]pyrimidines (**7a**) and (**7i**) suitable for single-crystal X-ray diffraction studies were grown from methanol. Crystallographic data and refinement results are summarized in Table 1 for **6a** and **6e** and in Table 2 for **7a** and **7i**. Full hemispheres of redundant diffracted intensities [5237 (**6a**), 5233 (**6e**), 5237 (**7a**), or 4438 (**7i**) 2−5 s frames for each with an ω- or ϕ-scan width of 0.50°] were measured at 100(2) K for single-domain specimens of all four compounds using monochromated Cu Kα radiation (λ = 1.54178 Å) on a dual-detector Bruker Proteum single crystal diffraction system equipped with Helios high-brilliance multilayer optics, an APEX II CCD (**6a**, **6e**, and **7a**) or Platinum 135 (**7i**) CCD detector and a Bruker MicroStar microfocus rotating anode X-ray source operating at 45 kV and 60 mA. Sample-to-detector distances of 50 mm (**6a**, **6e**, and **7a**) and 180 mm (**7i**) were used to collect data. Lattice constants were determined with the Bruker SAINT software package using peak centers for 9875 (**6a**), 9869 (**6e**), 8270 (**7a**), and 9796 (**7i**) reflections. Integrated reflection intensities were produced for all structures using the Bruker program SAINT[54] and the data were corrected empirically for variable absorption effects using equivalent reflections. The Bruker software package SHELXTL was used to solve the structure using "direct methods" techniques. All stages of weighted full-matrix least-squares refinement were conducted using F_o^2 data with the SHELXTL v2010.3-0 software package.[55]

The final structural models for all four structures incorporated anisotropic thermal parameters for all non-hydrogen atoms and isotropic thermal parameters for all

Scheme 1. Representative Classes of Compounds Containing the Pyrimidine Scaffold and Selected Molecular Targets of Acetylcholinesterase Inhibitors

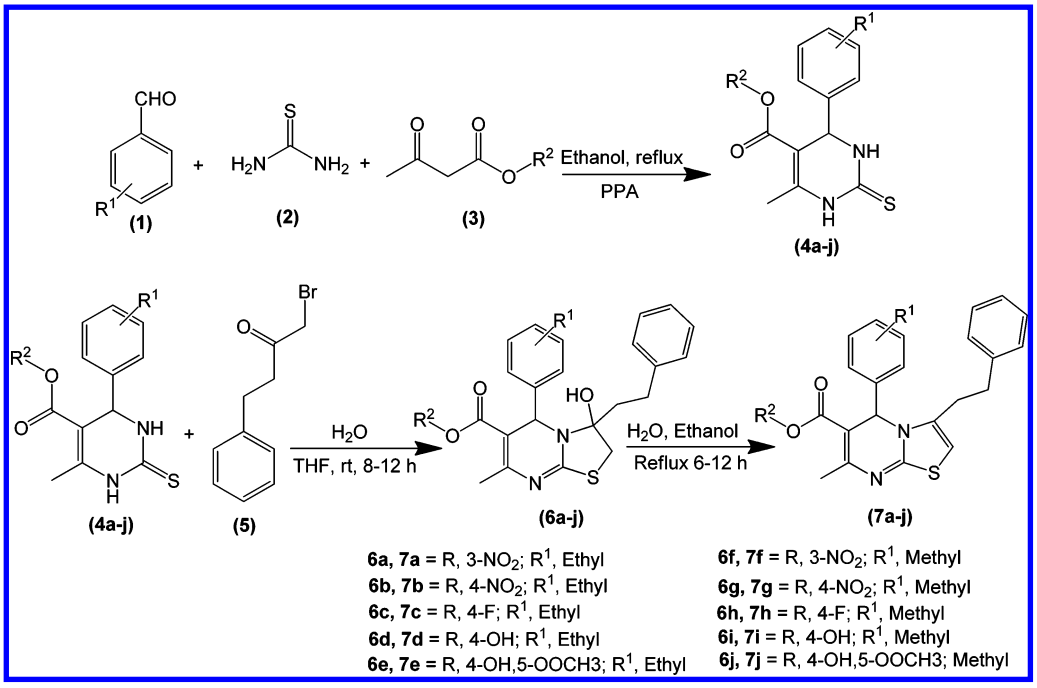

Scheme 2. Diastereomeric Representation of Compounds 6a−6j

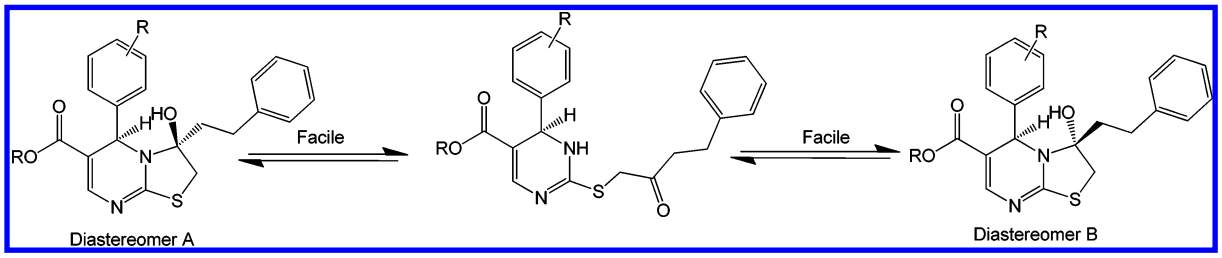

hydrogen atoms. All hydrogen atoms were located in a difference Fourier and then included in the structural model as individual isotropic atoms whose parameters were allowed to vary in least-squares refinement cycles. The methyl groups for **7i** were incorporated into the final structural model as rigid groups (using idealized sp^3-hybridized geometry and a C−H bond length of 0.98 Å) that were allowed to rotate freely about their C−C bonds in least-squares refinement cycles; the isotropic thermal parameters for the methyl hydrogen atoms were allowed to vary. The structures of **6a**, **6e**, **7a**, and **7i** are shown in Figures 1 and 2 and 4−6, respectively. Tables of fractional atomic coordinates, thermal parameters, bond lengths and angles, torsion angles, and hydrogen bonding parameters for the structures of **6a**, **6e**, **7a**, and **7i** are given in the Supporting Information.

3. RESULTS AND DISCUSSION

AChE Inhibitors Design. In order to develop drugs for Alzheimer's treatment,[56,57] a series of compounds were designed and their capacity to inhibit AChE activity was predicted by QSAR and molecular docking studies. Pharmacokinetic properties like absorption, distribution, metabolism, and excretion (ADME) were also defined to predict their adverse effects in the system. The QSAR analysis helped to derive highly applicable models that permitted the design of novel and

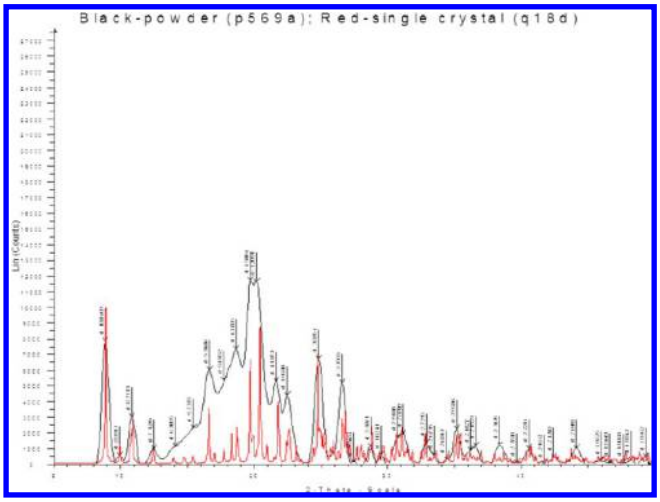

Figure 3. Superimposed experimental and calculated Cu Kα X-ray powder patterns for solids removed from evaporated solution for HBr salt of **6a**. Experimental PXRD of pulverized bulk solid (black) and PXRD calculated from single crystal structure determination (red) for HBr salt of **6a**.

reactive molecules.[57] Preliminary structure−activity relationship (SAR) studies indicated that the pyrimidine moiety is required for inhibition of AChE activity.[38,58] This is consistent with

dx.doi.org/10.1021/ci400196z | J. Chem. Inf. Model. 2013, 53, 2033−2046

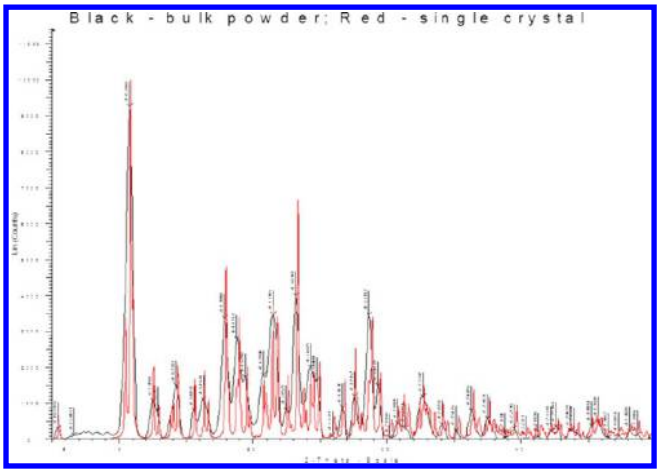

Figure 4. Superimposed experimental and calculated Cu Kα X-ray powder patterns for solids removed from evaporated solution for HBr salt of **6e**. Experimental PXRD of pulverized bulk solid (black) and PXRD calculated from single crystal structure determination (red) for HBr salt of **6e**.

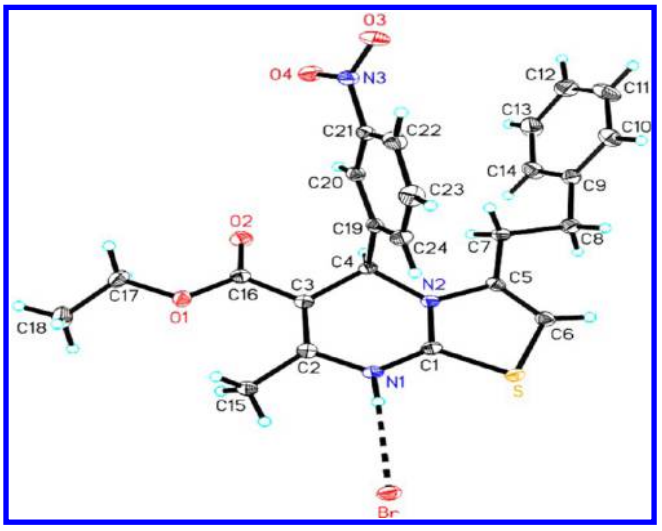

Figure 5. Crystal structure for HBr salt of **7a** showing 50% probability displacement ellipsoids and the atom-numbering scheme.

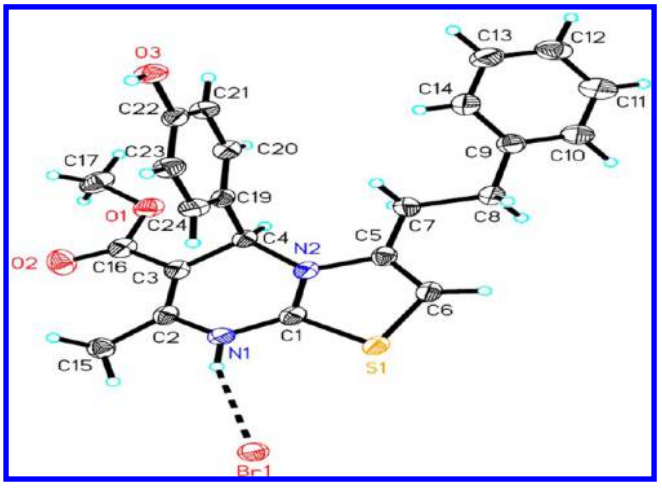

Figure 6. Crystal structure for HBr salt of **7i** showing 50% probability displacement ellipsoids and the atom-numbering scheme.

pyrimidine derivatives being widely used as treatment of AD at different stages.[38−41] Pyrimidine derivatives have been useful for treating diseases associated with the deposition of beta-amyloid peptide in the brain (such as Alzheimer's disease[39]) and as microtubule affinity regulating kinase inhibitors or in the treatment or prevention of tauopathies.

As acetylcholinesterase (AChE) plays a key role in the regulation of the cholinergic system, inhibition of AChE has emerged as one of the most promising strategies for the treatment of AD.[38,59−61] Pyrimidine derivatives were therefore built and screened virtually using the docking method.

The goal of the present work was to synthesize AChE inhibitor drugs with enhanced bioavailability by increasing the number of aromatic substituents on the basic pyrimidine core. This should increase affinity for the dual binding sites of AChE and increase the acetylcholine level in the brain. The *5H*-thiazolo[3,2-*a*]pyrimidines provide the minimum functionality necessary to achieve good binding deep in the AChE dual active site. Since pyrimidine species also provide remarkable enhancements of permeation across biological membranes and of oral bioavailability, we set out to design and synthesize small drug molecules incorporating substituted *2H*-thiazolo[3,2-*a*]pyrimidine and *5H*-thiazolo[3,2-*a*]pyrimidine moieties (Scheme 2) that might have the capacity to cross the blood−brain barrier (BBB) and inhibit AChE activity. To further enhance the potential for inhibition, *5H*-thiazolo[3,2-*a*]-pyrimidines were designed to incorporate significant intramolecular flexibility by linking polar groups having highly favorable enthalpic interactions with conserved enzyme residues in the dual binding site.

Chemistry. A series of novel *2H*-thiazolo[3,2-*a*]pyrimidine and *5H*-thiazolo[3,2-*a*]pyrimidine derivatives were synthesized with variations at the aromatic rings and their linking group. As shown in Scheme 2, various aromatic aldehydes, thiourea, and ethylacetoacetate/methylacetoacetate (**2**) were mixed with polyphosphoric acid (PPA) (5 mol %) in ethanol (10 mL) in a one-pot, three-component reaction. The reaction mixture was refluxed with stirring for 6−8 h. PPA is an extremely efficient catalyst for this reaction. All the reactions were carried out following this general procedure. On each occasion, the spectral data (IR, NMR, and HRMS) of prepared known compounds were identical with those reported in the literature. Further, the intermediate dihydropyrimidines **4a−4j** were reacted with 1-bromo-4-phenylbutan-2-one at room temperature for 6−12 h to give a solid. This was filtered and washed with water to obtain compounds **6a−6j** in high yields (80−95%; see Table 3). Since this resulted in diastereomers having two chiral centers i.e. **6a−6j**, we employed simple diastereomeric crystallization to separate them. Diastereomeric crystallization is used so widely that it provides a measure for judging alternative processes.[62] The salts formed are diastereomers with different physical properties and may be separated in a number of ways, for example by chromatography, but the most efficient method of separating such diastereomers is by crystallization. Many significant pharmaceuticals are resolved using diastereomeric crystallization.[62] This is a widely used technique in manufacturing processes for providing single-isomer drugs produced by synthetic means. A study of a representative group of market drugs shows that more than 65% are manufactured by methods involving diastereomeric crystallization of salts.[63,64]

We have preferentially isolated a single compound (diasteromer B) from the equilibrium shown in Scheme 2 using diastereomeric crystallization of the HBr salt (the HBr

dx.doi.org/10.1021/ci400196z | J. Chem. Inf. Model. 2013, 53, 2033−2046

Table 3. Synthesis of Tetrahydropyrimidine Derivatives

entry	R^1	R^2	reaction time (h)	yield (%)	melting points (°C) observed	melting points (°C) literature[a]
4a	3-NO_2	ethyl	4	87	204–206	206–207[70]
4b	4-NO_2	ethyl	5	88	110–111	111–112[71]
4c	4-F	ethyl	3	92	185–187	186–188[70]
4d	4-OH	ethyl	4.5	89	199–200	198–200[72]
4e	4-OH,5-$OOCH_3$	ethyl	8	87	239–240	
4f	3-NO_2	methyl	5	92	250–252	249–251[70]
4g	4-NO_2	methyl	6	94	205–207	204–207[70]
4h	4-F	methyl	4	91	184–186	183–184[70]
4i	4-OH	methyl	6	86	210–211	209–212[70]
4j	4-OH,5-$OOCH_3$	methyl	7	84	211–212	

[a]All the melting points were matched with the reported data.

Table 4. Definition of Descriptors

vsa_pol	approximation to the sum of VDW surface areas (Å^2) of polar atoms (atoms) that are both hydrogen bond donors and acceptors), such as −OH
vsa_hyd	approximation to the sum of VDW surface areas of hydrophobic atoms (Å^2)
VSA	van der Waals surface area; a polyhedral representation is used for each atom in calculating the surface area
zagreb	Zagreb index: the sum of d^2 over all heavy atoms i
WeinerPath	Wiener path number: half the sum of all the distance matrix entries as defined in the works of Balaban[73] and Wiener[74]
WeinerPol	half the sum of all distance matrix entries with a value of 3
vol	van der Waals volume calculated using a grid approximation (spacing 0.75 Å).

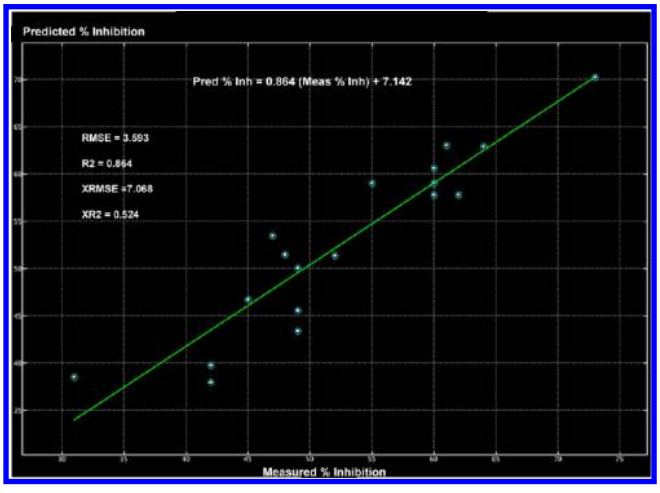

Figure 7. Linear correlation graph comparing a 20 compound training set of measured IC_{50}s with predicted values based on the calculated 2D QSAR regression model. The linearity of the training set model is shown with the values of the error (RMSE) and correlation factor (R^2) for both validated and cross-validated regressions.

was produced from the reaction of **4a**–**4j** with **5a**–**5j**). Salts **6a** and **6e** were the principal crystalline material that formed in methanol. This was verified by determining the solid-state structures for single crystals of **6a** and **6e** using X-ray diffraction (Table 1) and obtaining an experimental PXRD pattern for the bulk solid. This experimental powder pattern for the bulk was then compared with a calculated powder using atomic coordinates for the (single) crystal structures for **6a** and **6e** (Figures 1 and 2).

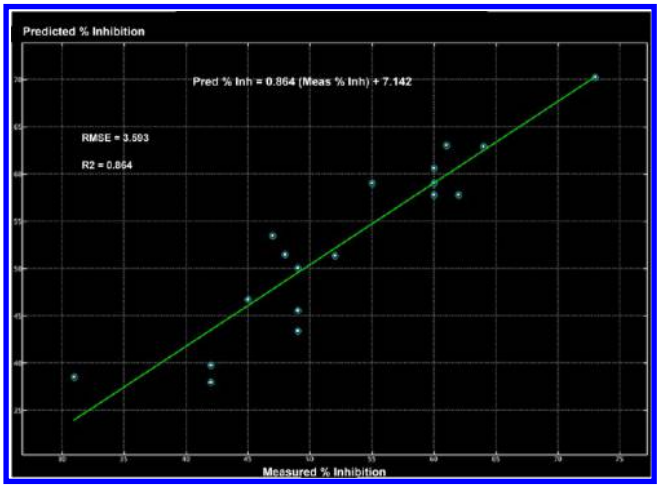

Figure 8. Linear correlation graph comparing a randomly selected 20 compound test set of measured IC_{50}s with predicted values based on the calculated 2D QSAR training set regression model. The linearity of the test model is shown with the values of the error (RMSE) and correlation factor (R^2).

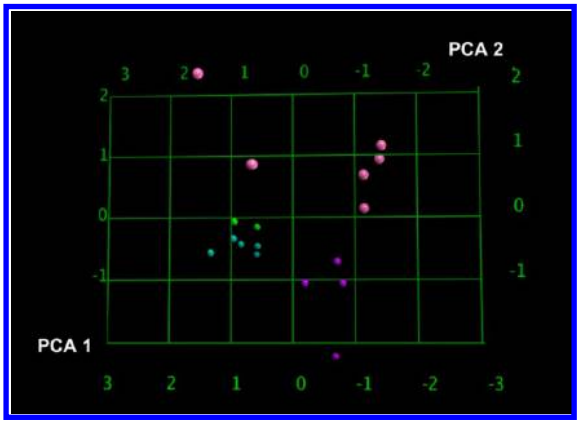

Figure 9. PCA plot of the training set of 20 AChE inhibitor compounds. The first two eigenvectors are shown (PCA1, PCA2) projected upon PCA3, which constituted 100% of the variance. The spheres indicate the position of each of the compounds within the set with measured activity (percent inhibition). On the basis of VSA, vol, vsa_pol, and zagreb descriptors, a clear separation between the top six active and less active candidates is observed within the region: PCA1 = −2 to +2, PCA2 > 0.

dx.doi.org/10.1021/ci400196z | J. Chem. Inf. Model. 2013, 53, 2033–2046

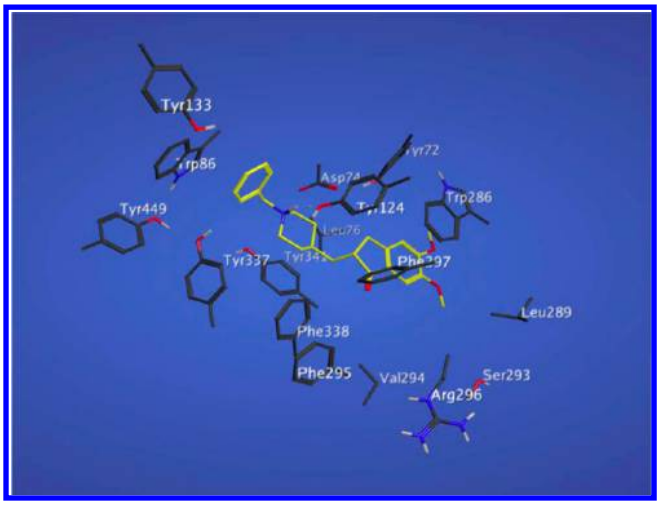

Figure 10. AChE active site for binding of donepezil is shown in yellow. Residues that contribute to its binding stabilization are indicated.

Table 5. Tabulation of Binding Affinities and Solvation Energies for Top Docking Candidates (6c, 7c, and 7h) Relative to Donepezil

compound	binding affinity (kcal/mol)	Born solvation energy (kcal/mol)
donepezil	−8.0 (0.3)	−28.2 (1.0)
compound **6c**	−8.3 (0.3)	−23.3 (1.0)
compound **7c**	−8.6 (0.3)	−24.9 (1.0)
compound **7h**	−8.3 (0.3)	−21.8 (1.0)

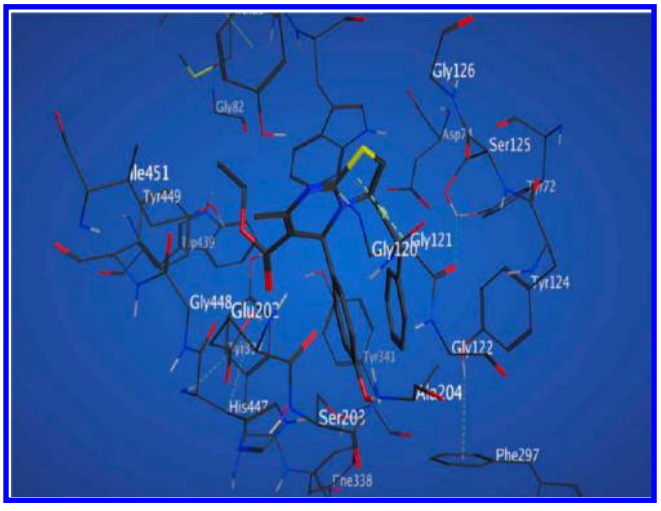

Figure 11. AChE active site for binding of lead candidate (compound **7c**), shown with bold bonds and standard colors for nonhydrogen atoms. Residues that contribute to its binding stabilization are indicated. The binding affinity (GBV!/WSA scoring function) was calculated as −8.6 (± 0.3)kcal/mol and Generalized Born solvation energy as −24.9(± 1.0).

Figures 3 and 4 each show a black experimental powder pattern for the dry bulk material from the crystallization vial that is superimposed with a red powder pattern calculated for the single crystal structures of compounds **6a** and **6e**, respectively. Each black pattern was obtained with some of the dry bulk solid from the crystallization vial that had been ground to a powder. Each red pattern was calculated with

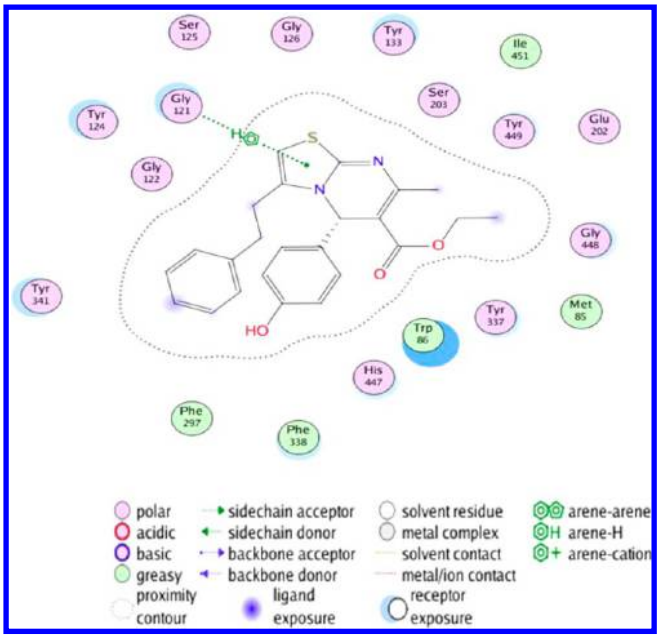

Figure 12. 2D ligand interaction diagram for lead candidate (compound **7c**), showing AChE residues important for binding stabilization. As indicated, arene-H-bonds, aromatic-stacking, and hydrophobic interactions play an import role in binding stabilization.

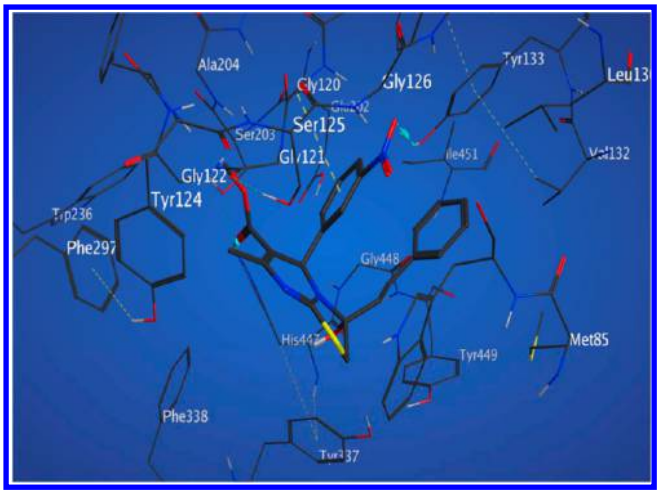

Figure 13. AChE active site for binding of lead candidate (compound **7h**), shown with bold bonds and standard colors for nonhydrogen atoms. Residues that contribute to its binding stabilization are indicated. The binding affinity (GBV!/WSA scoring function) was calculated as −8.3 (± 0.3) kcal/mol, and the Generalized Born solvation energy was −21.8 (± 1.0).

atomic coordinates resulting from the single crystal structure determination of compound **6a** or **6e** using the public-domain Mercury software package.[65] Clearly, the peaks for both sets of superimposed patterns occur at the same places and generally have the same relative heights. This indicates the significant presence of just one crystalline material (**6a** and **6e**) in the bulk solid that resulted when all of the solvent evaporated. Both bulk samples also contain a minor component that is an amorphous solid.

Compounds **6a**−**6j** were further refluxed for 6−8 h to form the compounds **7a**−**7j** in high yields. The synthetic route utilized to make our target "AChE inhibitors" compounds **6a**−**6j** and **7a**−**7j** is shown in Scheme 1. The chemical structures of

dx.doi.org/10.1021/ci400196z | J. Chem. Inf. Model. 2013, 53, 2033−2046

Figure 14. AChE active site for binding of lead candidate (compound **6c**), shown with bold bonds and standard colors for nonhydrogen atoms. Residues that contribute to its binding stabilization are indicated. The binding affinity (GBV!/WSA scoring function) was calculated as −8.3 (± 0.3)kcal/mol, and the Generalized Born solvation energy was −23.3 (± 1.0).

Figure 15. Compounds donepezil, **6c**, **7c**, and **7h** are shown in their docked position within the 1B41 structure. The peripheral active site (PAS) and catalytic active site (CAS) regions are indicated. The enzymatic triad (S203, H447, and E334) are shown relative to the docked potential candidates. Donepezil is shown in gray, compounds **6c** in yellow, **7c** in turquoise, and **7h** in magenta. All are nicely contained within the VDW surface defined by the AChE receptor.

the new compounds were confirmed by elemental analysis, IR, ^{1}H NMR, ^{13}C NMR spectral- and HRMS; the data are presented in the experimental section. Structures for compounds **6a**, **6e**, **7a** (Figure 5 and Table 2), and **7i** (Figure 6 and Table 2) were further confirmed by single crystal XRD.

QSAR Study. Three-dimensional structures were built for compounds **6a**−**6j** and **7a**−**7j** and optimized in a MOE working environment. Molecular dynamics simulations were carried out for each molecule and molecular descriptors were determined followed by QSAR linear regression study (Table 4). The correlation model showed a linear plot for both measured IC_{50} values and values predicted for the training set of molecules (Figure 7).[23,38,58,61] The correlation analysis showed an RMSD of 4.0 and r^2 value of 0.86. This linearity for

Table 6. Hits Determined by the Four Feature Pharmacophore Model

	mol	rmsd	mseq	$PRED_HITS	comp ID
1	fragment	0.8612	1	−15.2740	**6a**
2	fragment	0.7232	2	−8.0505	**6b**
3	fragment	0.6036	3	53.2487	**6c**
4	fragment	1.0910	4	29.4373	**6d**
5	fragment	0.5787	5	−13.5831	**6e**
6	fragment	0.8709	6	−32.6843	**6f**
7	fragment	0.9098	7	−24.8801	**6g**
8	fragment	0.6027	8	36.3966	**6h**
9	fragment	0.5879	9	−34.9239	**6j**
10	fragment	0.9033	10	59.6933	**7c**
11	fragment	0.8815	11	−10.4414	**7e**
12	fragment	0.8501	12	44.0813	**7h**
13	fragment	0.8418	13	−26.0600	**7j**

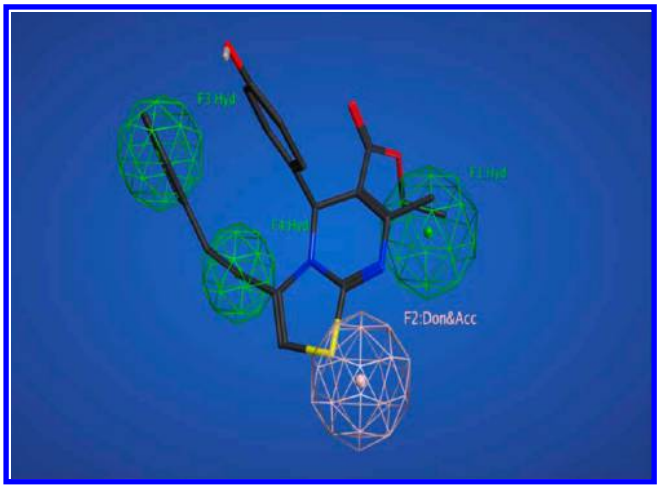

Figure 16. AChE pharmacophore model composed of the hydrophobic regions (Hyd) and H-bond donor/acceptor (Don and Acc). Compound **7c** is shown superimposed as occupying all four regions of the model.

the model indicates the reliability of QSAR to compare and predict the activity of a test set molecules (Figure 8).

QSAR Descriptors. *Principal Component Analysis.* A principal component analysis using the QSAR descriptors showed that the first two PCA eigenvectors included 100% of the variance. All the data values were found to lie in the range of −3 > PCA1 > +3 and −2 > PCA2 > +2, where each spot in the plot represents a molecule. Most interestingly, the most active compounds in our data set, as shown in magenta, are distinctly isolated from the other molecules within the region: 0 > PCA1 > 3.0 and 0.5 > PCA2 > −3.0 (Figure 9). This could provide an addition criterion for compound selection.

Molecular Docking of AChE Inhibitors. Molecular modeling has often been proven to be a powerful tool for rationalizing ligand−target interactions and for making this information available to virtual screening techniques. Molecular modeling studies were performed using human AChE, since they represent the pharmacological target for the development of new drugs for the treatment of AD. The crystal structure of AChE protein (1B41) was loaded into MOE (Molecular Operating Environment (MOE, version 2012.10)[27] with a resolution of 2.76 Å and a library was constructed for all the lead molecules.[66] The binding site of human AChE protein was identified from PDBSum,[67] and the residues D74, W86, N87,

dx.doi.org/10.1021/ci400196z | J. Chem. Inf. Model. 2013, 53, 2033−2046

Table 7. ADME Properties Predicted for 20 Novel Compounds

compound	[a]human intestinal absorption (%)	[b]in vitro Caco-2 cell permeability (nm/s)	[c]in vitro MDCK cell permeability (nm/s)	[d]in vitro plasma protein binding (%)	[e]in vivo blood−brain barrier penetration (C. brain/C. blood)
6a	97.561705	19.1355	0.105297	90.484755	0.0806771
6b	97.561705	7.97025	0.105297	90.142982	0.089125
6c	95.389128	31.8492	0.250481	88.226284	0.335066
6d	96.667520	51.638	0.301391	89.418601	0.150767
6e	96.493159	26.3461	0.065936	88.865351	0.0785162
6f	97.176050	19.8794	0.105973	91.276743	0.096315
6g	97.176050	9.71977	0.26827	90.909497	0.198659
6h	95.385717	28.8087	0.239105	88.468882	0.22168
6i	96.676358	49.1567	0.222715	89.696313	0.114523
6j	96.405668	24.6646	0.0872517	89.224416	0.0763619
7a	99.864657	37.971	0.120347	91.316081	0.453354
7b	99.864657	22.9359	0.120347	90.802189	0.487831
7c	96.628366	52.6213	0.407019	89.836610	0.153852
7d	97.487436	57.4001	0.727692	91.158003	0.201717
7e	97.687575	45.3655	0.0596721	89.703433	0.188834
7f	99.796273	35.696	0.102013	91.874991	0.464546
7g	99.796273	22.0079	0.34068	91.304055	0.739628
7h	96.60713	51.3119	0.281396	89.872761	0.140081
7i	97.466478	57.5096	0.380781	91.163376	0.222771
7j	97.820882	41.6557	0.0720615	89.912082	0.230354

[a]Human intestinal absorption is the sum of bioavailability and absorption evaluated from ratio of excretion or cumulative excretion in urine, bile, and feces. A value between 0 and 20% indicates poor absorption, 20−70% shows moderate absorption, and 70−100% indicates good absorption. [b]Caco-2 cells are derived from human colon adenocarcinoma and possess multiple drug transport pathways through the intestinal epithelium. A value <4 indicates low permeability, 4−70 shows middle permeability, and >70 indicates high permeability. [c]The MDCK cell system may be used as a good tool for rapid permeability screening. A value <25 indicates low permeability, 25−500 shows middle permeability, and >500 indicates high permeability. [d]The percent of drug binds to plasma protein. A value <90% indicates weak binding, and >90% indicates strong binding to plasma proteins. [e]BBB penetration is represented as BB = [brain]/[blood]. A value <0.1 indicates low absorption, 0.1−2.0 shows middle absorption, and >2.0 indicates higher absorption to the CNS.

G120, G121, G122, Y124, S125, G126, L130, E202, S203, F297, Y337, F338, Y341, H447, G448, and I451 were found to be interacting residues as shown in Figures 10−15.

Docking of Donepezil with AChE (1B41). As a validation of the docking procedure (Figure 10), the structure of the 1B41−donepezil complex was analyzed and the binding affinity (GBV/WSA scoring function) and Generalized Born solvation energy were calculated.

The binding affinity (GBV!/WSA scoring function) of donepezil was calculated as −8.0 (± 0.3) kcal/mol, and Generalized Born solvation energy as −28.2(± 1.0) kcal/mol. Donepezil therefore binds with >3 kcal/mol greater solvation energy than our predicted lead compounds, **6c**, **7c**, and **7h** (Table 5). Donepezil also has a 0.3−0.6 kcal/mol lower calculated affinity than compounds **6c**, **7c**, and **7h**, but this is within the 2σ limit. However donepizel has slightly higher solvation energy than the other compounds. It is tempting to suggest that it gains additional binding affinity by its desolvation stabilization within the aromatic lined "groove" site (PAS region) of the human AChE receptor, as compared to our inhibitor candidates.

Therefore, the docking procedure that was used gives us information about important ligand−receptor interactions and ligand affinities, using a protocol including molecular mechanics, genetic algorithm, and Lamarckian GA calculations. On the basis of the obtained hits, 5*H*-thiazolo[3,2-*a*]pyrimidine and 2*H*-thiazolo[3,2-*a*]pyrimidine derivatives emerged as promising candidates. Selected conformers of compounds were docked into the human AChE structure (PDB code 1B41), shown in Figures 11−15.

Among all docking conformations, compounds **7c** had the best least docking score of −8.6 kcal/mol and the next best docking scores were for compounds **6c** and **7h** with docking scores −8.3 and −8.3, respectively. **7c** was found to form an arene-hydrogen bond with Gly121. These three ligands had the first best least docking scores with stable ligand pose interactions in the docking sphere followed by the remaining lead compounds.

Pharmacophore Model. *AChE Inhibitor Four Feature Pharmacophore Model.* The pharmacophore model selected 13 out of 20 compounds in the database as hits (see Table 6). These are identified under "Comp ID". The column "$PRED_HITS" gives a calculated percent inhibition value from the QSAR model. The positive values are considered as active hits, which include compounds **6c**, **6d**, **6h**, **7c**, and **7h** (see Figure 16).

ADME Predictions.[68,69] ADME properties are important conditions and major parts of pharmacokinetics. Viable drugs should have perfect ADME properties for it to be approved as a drug in clinical tests. The ADME predictions of the present 20 compounds show satisfactory results. Among the 20, compounds **6a**−**6j** and **7a**−**7j** show good intestinal absorption. All of them show moderate permeability for in vitro Caco-2 cells and low permeability for in vitro MDCK cells. In vivo blood−brain barrier penetration capacity was predicted to have middle absorption to the CNS (central nervous system) for the compounds **6c**, **6g**, **6h**, and **7a**−**7j** whereas low absorption to the CNS was observed for the compounds **6a**, **6b**, **6d**, **6e**, **6f**, **6i**, and **6j**. Blood−brain barrier penetration is a crucial pharmacokinetic property because CNS-active compounds must pass across it and CNS-inactive compounds must not

dx.doi.org/10.1021/ci400196z | J. Chem. Inf. Model. 2013, 53, 2033−2046

pass across it to avoid CNS side effects. Generally, the degree to which any drug binds to plasma protein influences not only the drug action but also its disposition and efficacy. Usually, the drug that is unbound to plasma proteins will be available for diffusion or transport across cell membranes and thereby finally interact with the target. Herein with respect to ADME, the percent of drug bound with plasma proteins was predicted and the compounds **6a**−**6j** and **7a**−**7j** were predicted to bind strongly. The predicted ADME properties and their values are shown in Table 7.

4. CONCLUSIONS AND FUTURE DIRECTIONS

This study described the design, synthesis, diastereomeric crystallization, docking, 2D QSAR, and pharmacophore studies

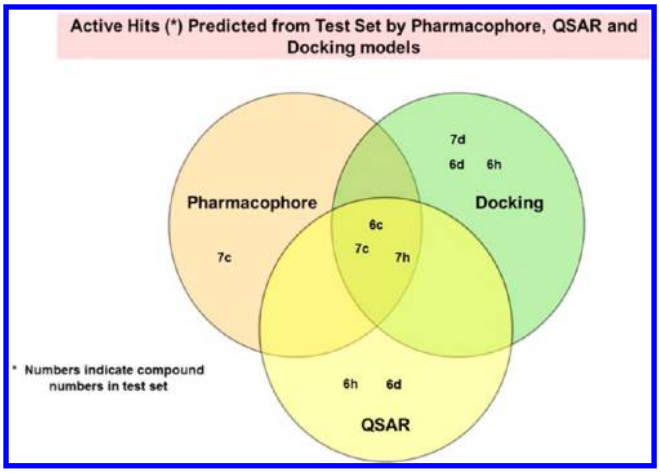

Figure 17. Union of predicted hits by QSAR, pharmacophore, and ligand docking with best ligands included in all three circles.

for a series of highly selective inhibitors of AChE. The pharmacophore model reflected the binding mode and important interactions of the ligands binding to the dual site of the enzyme. The ligand-oriented study used multiple contributions of ligand features to build a quantitative pharmacophore model from a training set of 20 AChE inhibitors with known IC_{50} values. The best pharmacophore model contained four basic pharmacophore features with a correlation coefficient of 0.90: two hydrogen bond acceptors and two hydrophobic interactions. This pharmacophore model was then applied to the novel set of 20 test molecules that have been synthesized and described in the Chemistry section. Taken individually, the docking, 2D QSAR and pharmacophore studies for the test set each indicated that at least 6 of the 20 test compounds should be reasonable inhibitors of AChE. All test compounds showed proper druglike 2D QSAR and ADMET properties. The ligand−protein complexes generated with molecular docking indicated that the six of the test molecules should be good AChE inhibitors since they showed good binding affinity with the dual sites of the enzyme receptor. Five of the 20 had good QSAR values, and 4 of the 20 had good pharmacophore values. However, only 3 of the 20 test compounds (**6c**, **7c**, and **7h**) had good docking, QSAR, and pharmacophore values, Figure 17. It therefore seems that by combining all three of these evaluation procedures, large numbers of new compounds can be screened as possible inhibitors of AChE. Since the present results indicate that compounds **6c**, **7c**, and **7h** should be excellent candidates for inhibition of AChE, we plan to use them as a starting point for developing even more potent analogues for the treatment of the Alzheimer's disease.

■ ASSOCIATED CONTENT

Supporting Information

Experimental details and spectroscopic data of synthesized compounds, ^{1}H, ^{13}C NMR chromatograms, and crystal structure supporting tables. This material is available free of charge via the Internet at http://pubs.acs.org.

■ AUTHOR INFORMATION

Corresponding Author

*Mailing address: 2099 Constant Avenue, University of Kansas, Lawrence, KS 66047. E-mail: shidu@ku.edu.

Notes

The authors declare no competing financial interest.

■ ACKNOWLEDGMENTS

This study was supported by grant awards (RO1GM095355 and R37AG037319) from the National Institute of General Medical Sciences and the National Institute on Aging. The authors thank the National Science Foundation (grant CHE-0923449) and the University of Kansas for funds to purchase the X-ray instrumentation and computers.

■ ABBREVIATIONS

AChE, acetylcholinesterases; ACh, acetylcholine; AD, Alzheimer's disease; AChEIs, acetylcholinesterase inhibitors; Aβ, amyloid beta; QSAR, quantitative structure−activity relationship; CoMFA, comparative molecular field analysis; ADMET, absorption, distribution, metabolism, and excretion and toxicity; FDA, Food and Drug Administration; BBB, blood−brain barrier; Caco2, human colon adenocarcinoma; MDCK, Madin−Darby canine kidney; SAR, structure−activity relationship; CNS, central nervous system; MOE, molecular operating environment; RMSE, root mean square error; PCA, principal component analysis; PDB, Protein Data Bank; MMFF94x, The Merck Molecular Force Field

■ REFERENCES

(1) Berman, H. M.; Bhat, T. N.; Bourne, P. E.; Feng, Z.; Gilliland, G.; Weissig, H.; Westbrook, J. The Protein Data Bank and the challenge of structural genomics. *Nat. Struct. Biol.* **2000**, *7* (Suppl), 957−9.

(2) Berman, H. M.; Westbrook, J.; Feng, Z.; Gilliland, G.; Bhat, T. N.; Weissig, H.; Shindyalov, I. N.; Bourne, P. E. The Protein Data Bank. *Nucleic. Acids. Res.* **2000**, *28*, 235−42.

(3) Dastmalchi, S.; Hamzeh-Mivehroud, M.; Ghafourian, T.; Hamzeiy, H. Molecular modeling of histamine H3 receptor and QSAR studies on arylbenzofuran derived H3 antagonists. *J. Mol. Graph. Model.* **2008**, *26*, 834−844.

(4) Glaser, B. Psychiatry and paedophilia: a major public health issue. *Aust. N. Z. J. Psychiatry.* **1998**, *32*, 162−7.

(5) Hauptmann, S.; Scherping, I.; Drose, S.; Brandt, U.; Schulz, K. L.; Jendrach, M.; Leuner, K.; Eckert, A.; Muller, W. E. Mitochondrial dysfunction: an early event in Alzheimer pathology accumulates with age in AD transgenic mice. *Neurobiol. Aging.* **2009**, *30*, 1574−86.

(6) Mao, Y.; Shang, Z.; Imai, Y.; Hoshino, T.; Tero, R.; Tanaka, M.; Yamamoto, N.; Yanagisawa, K.; Urisu, T. Surface-induced phase separation of a sphingomyelin/cholesterol/ganglioside GM1-planar bilayer on mica surfaces and microdomain molecular conformation that accelerates Abeta oligomerization. *Biochim. Biophys. Acta* **2010**, *1798*, 1090−1099.

(7) Park, S. K.; Pegan, S. D.; Mesecar, A. D.; Jungbauer, L. M.; LaDu, M. J.; Liebman, S. W. Development and validation of a yeast high-throughput screen for inhibitors of Abeta(4)(2) oligomerization. *Dis. Model. Mech.* **2011**, *4*, 822−831.
(8) Stains, C. I.; Ghosh, I. When conjugated polymers meet amyloid fibrils. *ACS. Chem. Biol.* **2007**, *2*, 525−528.
(9) Sun, F.; Knebelmann, B.; Pueyo, M. E.; Zouali, H.; Lesage, S.; Vaxillaire, M.; Passa, P.; Cohen, D.; Velho, G.; Antignac, C.; et al. Deletion of the donor splice site of intron 4 in the glucokinase gene causes maturity-onset diabetes of the young. *J. Clin. Invest.* **1993**, *92*, 1174−1180.
(10) Alipour, M.; Khoobi, M.; Foroumadi, A.; Nadri, H.; Moradi, A.; Sakhteman, A.; Ghandi, M.; Shafiee, A. Novel coumarin derivatives bearing N-benzyl pyridinium moiety: Potent and dual binding site acetylcholinesterase inhibitors. *Bioorg. Med. Chem.* **2012**, *20*, 7214−7222.
(11) Alipour, M.; Khoobi, M.; Foroumadi, A.; Nadri, H.; Moradi, A.; Sakhteman, A.; Ghandi, M.; Shafiee, A. Novel coumarin derivatives bearing N-benzyl pyridinium moiety: Potent and dual binding site acetylcholinesterase inhibitors. *Bioorg. Med. Chem.* **2012**, *20*, 7214−22.
(12) Yankner, B. A.; Duffy, L. K.; Kirschner, D. A. Neurotrophic and Neurotoxic Effects of Amyloid Beta-Protein - Reversal by Tachykinin Neuropeptides. *Science* **1990**, *250*, 279−282.
(13) Iijima, K.; Liu, H. P.; Chiang, A. S.; Hearn, S. A.; Konsolaki, M.; Zhong, Y. Dissecting the pathological effects of human A beta 40 and A beta 42 in Drosophila: A potential model for Alzheimer's disease. *Proc. Natl. Acad. Sci. U.S.A.* **2004**, *101*, 6623−6628.
(14) Tabet, N. Acetylcholinesterase inhibitors for Alzheimer's disease: anti-inflammatories in acetylcholine clothing! *Age. Ageing* **2006**, *35*, 336−338.
(15) Bolognesi, M. L.; Andrisano, V.; Bartolini, M.; Banzi, R.; Melchiorre, C. Propidium-based polyamine ligands as potent inhibitors of acetylcholinesterase and acetylcholinesterase-induced amyloid-beta aggregation. *J. Med. Chem.* **2005**, *48*, 24−27.
(16) Savini, L.; Gaeta, A.; Fattorusso, C.; Catalanotti, B.; Campiani, G.; Chiasserini, L.; Pellerano, C.; Novellino, E.; McKissic, D.; Saxena, A. Specific targeting of acetylcholinesterase and butyrylcholinesterase recognition sites. Rational design of novel, selective, and highly potent cholinesterase inhibitors. *J. Med. Chem.* **2003**, *46*, 1−4.
(17) Francis, P. T.; Palmer, A. M.; Snape, M.; Wilcock, G. K. The cholinergic hypothesis of Alzheimer's disease: a review of progress. *J. Neuro. Neurosur. Psy.* **1999**, *66*, 137−147.
(18) Allen, N. H. P.; Burns, A. The Treatment of Alzheimers-Disease. *J. Psychopharmacol.* **1995**, *9*, 43−56.
(19) Ibach, B.; Haen, E. Acetylcholinesterase inhibition in Alzheimer's disease. *Cur. Pharma. Des.* **2004**, *10*, 231−251.
(20) Birks, J. Cholinesterase inhibitors for Alzheimer's disease. *Cochrane Database System. Rev.* **2006**, *1*, CD005593.
(21) Wilcock, G.; Howe, I.; Coles, H.; Lilienfeld, S.; Truyen, L.; Zhu, Y.; Bullock, R.; Grp, G. G. S. A long-term comparison of galantamine and donepezil in the treatment of Alzheimer's disease. *Drugs Aging* **2003**, *20*, 777−789.
(22) Bullock, R.; Touchon, J.; Bergman, H.; Gambina, G.; He, Y. S.; Rapatz, G.; Nagel, J.; Lane, R. Rivastigmine and donepezil treatment in moderate to moderately-severe Alzheimer's disease over a 2-year period. *Cur. Med. Res. Opin.* **2005**, *21*, 1317−1327.
(23) Birks, J.; Harvey, R. J. Donepezil for dementia due to Alzheimer's disease (Review). *Cochrane Database System. Rev.* **2006**, *25*, CD001190.
(24) Loy, C.; Schneider, L. Galantamine for Alzheimer's disease and mild cognitive impairment. *Cochrane Database System. Rev.* **2006**, *25*, CD001747.
(25) Birks, J.; Evans, J. G.; Iakovidou, V.; Tsolaki, M.; Holt, F. E. Rivastigmine for Alzheimer's disease. *Cochrane Database System. Rev.* **2000**, *4*, CD001191.
(26) Raves, M. L.; Harel, M.; Pang, Y. P.; Silman, I.; Kozikowski, A. P.; Sussman, J. L. Structure of acetylcholinesterase complexed with the nootropic alkaloid, (-)-huperzine A. *Nat. Struct. Biol.* **1997**, *4*, 57−63.
(27) Chemical computing group releases MOE version 2002.03. *J. Chem. Educ.* **2002**, *79*, 951−951.
(28) Abad, N. H.; Doulatabad, N. S.; Mohammadi, A.; Srazi, H. R. Treatment of Visual Hallucinations in Schizophrenia by Acetylcholinesterase Inhibitors: a case report. *Iran. J. Psychiatry.* **2011**, *6*, 161−163.
(29) Park, S. K.; Pegan, S. D.; Mesecar, A. D.; Jungbauer, L. M.; Ladu, M. J.; Liebman, S. W. Development and validation of a yeast high-throughput screen for inhibitors of A beta(42) oligomerization. *Dis. Model. Mech.* **2011**, *4*, 822−831.
(30) Stains, C. I.; Ghosh, I. When conjugated polymers meet amyloid fibrils. *ACS. Chem. Biol.* **2007**, *2*, 525−528.
(31) Mori, F.; Lai, C. C.; Fusi, F.; Giacobini, E. Cholinesterase-Inhibitors Increase Secretion of Apps in Rat-Brain Cortex. *Neuroreport* **1995**, *6*, 633−636.
(32) Giacobini, E. Cholinesterases: New roles in brain function and in Alzheimer's disease. *Neurochem. Res.* **2003**, *28*, 515−522.
(33) Francis, P. T.; Nordberg, A.; Arnold, S. E. A preclinical view of cholinesterase inhibitors in neuroprotection: do they provide more than symptomatic benefits in Alzheimer's disease? *Trends Pharmacol. Sci.* **2005**, *26*, 104−111.
(34) Hardy, J.; Selkoe, D. J. Medicine - The amyloid hypothesis of Alzheimer's disease: Progress and problems on the road to therapeutics. *Science* **2002**, *297*, 353−356.
(35) Selkoe, D. J. Normal and Abnormal Biology of the Beta-Amyloid Precursor Protein. *Annu. Rev. Neurosci.* **1994**, *17*, 489−517.
(36) Inestrosa, N. C.; Alvarez, A.; Perez, C. A.; Moreno, R. D.; Vicente, M.; Linker, C.; Casanueva, O. I.; Soto, C.; Garrido, J. Acetylcholinesterase accelerates assembly of amyloid-beta-peptides into Alzheimer's fibrils: Possible role of the peripheral site of the enzyme. *Neuron* **1996**, *16*, 881−891.
(37) Castro, A.; Martinez, A. Peripheral and Dual Binding Site Acetylcholinesterase Inhibitors: Implications in treatment of Alzheimer's Disease. *Mini-Rev. Med. Chem.* **2001**, *1*, 267−272.
(38) Zhi, H.; Chen, L. M.; Zhang, L. L.; Liu, S. J.; Wan, D. C. C.; Lin, H. Q.; Hu, C. Design, synthesis, and biological evaluation of 5H-thiazolo[3,2-a]pyrimidine derivatives as a new type of acetylcholinesterase inhibitors. *Arkivoc* **2008**, 266−277.
(39) Rivkin, A.; Ahearn, S. P.; Chichetti, S. M.; Kim, Y. R.; Li, C. M.; Rosenau, A.; Kattar, S. D.; Jung, J.; Shah, S.; Hughes, B. L.; Crispino, J. L.; Middleton, R. E.; Szewczak, A. A.; Munoz, B.; Shearman, M. S. Piperazinyl pyrimidine derivatives as potent gamma-secretase modulators. *Bioorg. Med. Chem. Lett.* **2010**, *20*, 1269−1271.
(40) Messer, W. S., Jr.; Rajeswaran, W. G.; Cao, Y.; Zhang, H. J.; el-Assadi, A. A.; Dockery, C.; Liske, J.; O'Brien, J.; Williams, F. E.; Huang, X. P.; Wroblewski, M. E.; Nagy, P. I.; Peseckis, S. M. Design and development of selective muscarinic agonists for the treatment of Alzheimer's disease: characterization of tetrahydropyrimidine derivatives and development of new approaches for improved affinity and selectivity for M1 receptors. *Pharm. Acta. Helv.* **2000**, *74*, 135−40.
(41) Kypta, R. M. GSK-3 inhibitors and their potential in the treatment of Alzheimer's disease. *Exp. Opin. Ther. Patents* **2005**, *15*, 1315−1331.
(42) Rivkin, A.; Ahearn, S. P.; Chichetti, S. M.; Kim, Y. R.; Li, C. M.; Rosenau, A.; Kattar, S. D.; Jung, J.; Shah, S.; Hughes, B. L.; Crispino, J. L.; Middleton, R. E.; Szewczak, A. A.; Munoz, B.; Shearman, M. S. Piperazinyl pyrimidine derivatives as potent gamma-secretase modulators. *Bioorg. Med. Chem. Lett.* **2010**, *20*, 1269−1271.
(43) Timm, T.; von Kries, J. P.; Li, X. Y.; Zennpel, H.; Mandelkow, E.; Mandelkow, E. M. Microtubule Affinity Regulating Kinase Activity in Living Neurons Was Examined by a Genetically Encoded Fluorescence Resonance Energy Transfer/Fluorescence Lifetime Imaging-based Biosensor Inhibitors with Therapeutic Potential. *J. Biol. Chem.* **2011**, *286*, 41711−41722.
(44) Ono, M.; Hayashi, S.; Matsumura, K.; Kimura, H.; Okamoto, Y.; Ihara, M.; Takahashi, R.; Mori, H.; Saji, H. Rhodanine and Thiohydantoin Derivatives for Detecting Tau Pathology in Alzheimer's Brains. *ACS Chem. Neurosci.* **2011**, *2*, 269−275.

(45) Heritage, T. W.; Ferguson, A. M.; Turner, D. B.; Willett, P. EVA: A novel theoretical descriptor for QSAR studies. *Persp. Drug Discov. Des.* **1998**, *9*−*11*, 381−398.
(46) Todeschini, R.; Gramatica, P. New 3D molecular descriptors: The WHIM theory and QSAR applications. *Perspect. Drug Discov. Des.* **1998**, *9*−*11*, 355−380.
(47) Vilar, S.; Cozza, G.; Moro, S. Medicinal Chemistry and the Molecular Operating Environment (MOE): Application of QSAR and Molecular Docking to Drug Discovery. *Cur. Top. Med. Chem.* **2008**, *8*, 1555−1572.
(48) Irvine, J. D.; Takahashi, L.; Lockhart, K.; Cheong, J.; Tolan, J. W.; Selick, H. E.; Grove, J. R. MDCK (Madin-Darby canine kidney) cells: A tool for membrane permeability screening. *J. Pharm. Sci.* **1999**, *88*, 28−33.
(49) Zhao, Y. H.; Le, J.; Abraham, M. H.; Hersey, A.; Eddershaw, P. J.; Luscombe, C. N.; Butina, D.; Beck, G.; Sherborne, B.; Cooper, I.; Platts, J. A. Evaluation of human intestinal absorption data and subsequent derivation of a quantitative structure-activity relationship (QSAR) with the Abraham descriptors. *J. Pharm. Sci.* **2001**, *90*, 749−84.
(50) Vilar, S.; Cozza, G.; Moro, S. Medicinal chemistry and the molecular operating environment (MOE): application of QSAR and molecular docking to drug discovery. *Cur. Top. Med. Chem.* **2008**, *8*, 1555−72.
(51) Vilar, S.; Gonzalez-Diaz, H.; Santana, L.; Uriarte, E. QSAR model for alignment-free prediction of human breast cancer biomarkers based on electrostatic potentials of protein pseudofolding HP-lattice networks. *J. Comput. Chem.* **2008**, *29*, 2613−22.
(52) Yao, J.; Irwin, R. W.; Zhao, L.; Nilsen, J.; Hamilton, R. T.; Brinton, R. D. Mitochondrial bioenergetic deficit precedes Alzheimer's pathology in female mouse model of Alzheimer's disease. *Proc. Natl. Acad. Sci. U.S.A.* **2009**, *106*, 14670−5.
(53) Data Collection: *SMART Software in APEX2 v2010.3-0 Suite*; Bruker-AXS: Madison, WI; 2010.
(54) Data Reduction: *SAINT Software in APEX2 v2010.3-0 Suite*; Bruker-AXS: Madison, WI, 2010.
(55) Refinement: *SHELXTL v2010.3-0*; Bruker-AXS: Madison, WI, 2010.
(56) Xie, Y.; Deng, S.; Chen, Z.; Yan, S.; Landry, D. W. Identification of small-molecule inhibitors of the Abeta-ABAD interaction. *Bioorg. Med. Chem. Lett.* **2006**, *16*, 4657−60.
(57) Valasani, K. R.; Hu, G.; Chaney, M. O.; Yan, S. S. Structure-Based Design and Synthesis of Benzothiazole Phosphonate Analogues with Inhibitors of Human ABAD-Abeta for Treatment of Alzheimer's Disease. *Chem. Biol. Drug. Des.* **2012**, *81*, 238−349.
(58) Zhi, H.; Chen, L. M.; Zhang, L. L.; Liu, S. J.; Wan, D. C. C.; Lin, H. Q.; Hu, C. Design, Synthesis, and Biological Evaluation of 5H-Thiazolo[3,2-a]pyrimidine-6-carboxylic Acid Ethyl Ester Derivatives as a Novel Series of Acetylcholinesterase Inhibitors. *Chem. Res. Chin. Univ.* **2009**, *25*, 332−337.
(59) Dorronsoro, I.; Castro, A.; Martinez, A. Peripheral and dual binding site inhibitors of acetylcholinesterase as neurodegenerative disease-modifying agents. *Exp. Opin. Ther. Patents* **2003**, *13*, 1725−1732.
(60) Ma, H. J.; Xie, R. L.; Zhao, Q. F.; Mei, X. D.; Ning, J. Synthesis and Insecticidal Activity of Novel Carbamate Derivatives as Potential Dual-Binding Site Acetylcholinesterase Inhibitors. *J. Agri. Food. Chem.* **2010**, *58*, 12817−12821.
(61) Leonetti, F.; Cappa, A.; Maccallini, C.; Carotti, A. Synthesis of potential dual binding site acetylcholinesterase inhibitors through an efficient solid phase approach based on the Mitsunobu reaction. *Arkivoc* **2004**, 272−285.
(62) Ruano, J. L. G.; Rodriguez, J.; Alcudia, F.; Llera, J. M.; Olefirowicz, E. M.; Eliel, E. L. Conformational-Analysis 0.47. The Stereochemistry of Sulfur Organic-Compounds 0.21. The Conformation of Oxanes with Sulfur Substituents. *J. Org. Chem.* **1987**, *52*, 4099−4107.
(63) Ahuja, S. Are chiral separations of drugs really easy? *Abstr. Pap. Am. Chem. Soc.* **2007**, 234.
(64) Ahuja, S. Chiral Separations - an Overview. In *Chiral Separations by Liquid Chromatography*; ACS Symposium Series; American Chemical Society: Washington, D.C., 1991; Vol. *471*, pp 1−26.
(65) Macrae, C. F.; Bruno, I. J.; Chisholm, J. A.; Edgington, P. R.; McCabe, P.; Pidcock, E.; Rodriguez-Monge, L.; Taylor, R.; van de Streek, J.; Wood, P. A. Mercury CSD 2.0 - new features for the visualization and investigation of crystal structures. *J. Appl. Crystallogr.* **2008**, *41*, 466−470.
(66) Davies, R. J.; Pierce, A. C.; Forster, C.; Grey, R.; Xu, J.; Arnost, M.; Choquette, D.; Galullo, V.; Tian, S. K.; Henkel, G.; Chen, G.; Heidary, D. K.; Ma, J.; Stuver-Moody, C.; Namchuk, M. Design, synthesis, and evaluation of a novel dual FMS-like tyrosine kinase 3/stem cell factor receptor (FLT3/c-KIT) inhibitor for the treatment of acute myelogenous leukemia. *J. Med. Chem.* **2011**, *54*, 7184−92.
(67) Laskowski, R. A. PDBsum: summaries and analyses of PDB structures. *Nucleic Acids Res.* **2001**, *29*, 221−2.
(68) Crivori, P.; Cruciani, G.; Carrupt, P. A.; Testa, B. Predicting blood-brain barrier permeation from three-dimensional molecular structure. *J. Med. Chem.* **2000**, *43*, 2204−2216.
(69) Nielsen, P. A.; Andersson, O.; Hansen, S. H.; Simonsen, K. B.; Andersson, G. Models for predicting blood-brain barrier permeation. *Drug Discov. Today* **2011**, *16*, 472−475.
(70) Liu, Q. J.; Pan, N.; Xu, J. H.; Zhang, W. W.; Kong, F. P. Microwave-Assisted and Iodine-Catalyzed Synthesis of Dihydropyrimidin-2-Thiones Via Biginelli Reaction under Solvent-Free Conditions. *Synth. Commun.* **2013**, *43*, 139−146.
(71) Lu, J.; Ma, H. R. Iron(III)-catalyzed synthesis of dihydropyrimidinones. Improved conditions for the Biginelli reaction. *Synlett* **2000**, *1*, 63−64.
(72) Wang, Z. T.; Xu, L. W.; Xia, C. G.; Wang, H. Q. Novel Biginelli-like three-component cyclocondensation reaction: efficient synthesis of 5-unsubstituted 3,4-dihydropyrimidin-2(1H)-ones. *Tetrahedron Lett.* **2004**, *45*, 7951−7953.
(73) Balaban, A. T. Five New Topological Indices for the Branching of Tree-Like Graphs. *Theor. Chim. Acta* **1979**, *53*, 355−375.
(74) Wiener, H. Structural Determination of Paraffin Boiling Points. *J. Am. Chem. Soc.* **1974**, *69*, 17−20.